Investigation of the Protolytic Equilibrium of a Highly Brønsted Acidic Ionic Liquid and Residual Water using Raman Spectroscopy

Yingzhen Chen,[1,2] Manuel B. Endres,[1] Jürgen Giffin,[1] and Carsten Korte*[1,2]

[1] Institute of Energy and Climate Research – Electrochemical Process Engineering (IEK-14), Forschungszentrum Jülich GmbH, 52428 Jülich, Germany

[2] RWTH Aachen University, 52062 Aachen, Germany

Abstract

Protic ionic liquids (PILs) are promising candidates as non-aqueous proton-conducting electrolytes for use in polymer electrolyte membrane fuel cells with operating temperatures over 100 °C. 2-sulfoethylammonium triflate [2-Sea][TfO] is one such PIL electrolyte, in which the highly Brønsted acidic sulfoalkylammonium cations act as mobile protonic charge carriers and proton donors. In order to gain a molecular-level understanding of proton transfer in a PIL electrolyte containing a small amount of residual water from fuel cell operation, the protolytic equilibrium of the highly acidic cation was investigated by means of Raman spectroscopy. Density functional theory (DFT) calculations were conducted to identify the vibration modes sensitive to protonation and to gain information on the possible conformation of the cation. The deprotonation of the 2-sulfoethylammonium cation resulted in a characteristic upward frequency shift in the ν(SC) stretching vibration. An equilibrium constant of 0.23 ± 0.09 was calculated for the protolytic reaction, indicating [2-Sea][TfO] as a promising proton donor for the fuel cell application.

Keywords: Protic ionic liquid; Non-aqueous electrolytes; Protolytic equilibrium; Residual water; Raman spectroscopy;

1 Introduction

Atmospheric operation of a polymer electrolyte fuel cell (PEFC) at elevated temperatures above 100 °C has several advantages: *i*) no feed gas humidification and water recirculation is needed; *ii*) more efficient heat management (a smaller cooling system, recovering high-grade waste heat); and *iii*) a higher tolerance against feed gas impurities [1–3]. However, the use of proton exchange membranes based on sulfonated fluoropolymers, such as NAFION® or AQUIVION®, limit the operating temperature to below 80 °C (ambient pressure) because the proton conductivity relies on the uptake of water. Protic ionic liquids (PILs) immobilized in a host membrane material constitute promising candidates for proton-conducting electrolytes for fuel cells operated above 100 °C [4].

An ionic liquid generally consists of bulky cations and counter anions, resulting in a low-lattice energy and thus a melting point close to room temperature. In a PIL, the cation or anion are able to function as a proton donor and carrier, respectively. A PIL with an acidic cation BH^+ can be prepared by a protolytic reaction between an (organic) base B and a super acid HA (1:1 stoichiometry) [5]:

$$B + HA \rightarrow BH^+ + A^- \quad (1)$$

PILs of BH^+A^- type are intrinsic proton conductors. In non-aqueous protic electrolytes—as the solvent is no longer available as an omni-present proton donor—the cation BH^+ acts as mobile protonic charge carriers and underlies a vehicular transport mechanism [6]. PILs are usually miscible with water and tend to absorb it from the air due to their high-polarity character. Under the operating conditions of a fuel cell, the amphoteric H_2O, as well as the free base B, is continually electrochemically produced on the cathode side:

$$2\ BH^+ + 1/2\ O_2 + 2\ e^- \rightarrow 2\ B + H_2O \quad (2)$$

Thus, a certain steady state content of water should be taken into consideration when using a PIL as an electrolyte in a fuel cell at even elevated temperatures. Former studies show that the addition of water to an ionic liquid enhances the ion conductivity and improves the oxygen reduction reaction (ORR) kinetics [7]. An ^{1}H-PFG-NMR study on PILs demonstrates a transition between vehicular and cooperative proton transport depending on the concentration of residual water and the cation acidity [8].

PILs with a sulfoalkylammonium cation ($NH_3^+(CH_2)_nSO_3H$) have recently been suggested for potential PEFC applications. The high acidic cation can act as a strong proton donor in the ORR [9]. 2-Sulfoethylammonium triflate ([2-Sea][TfO]) was selected for investigation in this work as a model of such PILs. In a recent study, we found that [2-Sea][TfO] exhibits extraordinary electrochemical properties. Its ORR kinetic current density of 95 wt% [2-Sea][TfO] at 0.8 V *vs.* NHE at 110 °C is about five times higher than equiconcentrated H_3PO_4. At 100 °C, a total conductivity of ∼2.5 mS cm^{-1} is reached [10]. This PIL can be prepared via a protolysis reaction of the weak zwitterionic Brønsted base taurine and trifluoromethanesulfonic acid CF_3SO_3H:

$$NH_3^+(CH_2)_2SO_3^- + CF_3SO_3H \rightarrow NH_3^+(CH_2)_2SO_3H + CF_3SO_3^- \quad (3)$$

The resulting PIL consists of $[2\text{-Sea}]^+$ cations and triflate anions $[TfO]^-$. In contrast to the findings of many studies on the acidity of taurine, there is only little data available on the acidity of the $[2\text{-Sea}]^+$ cation, *i.e.*, on the strength of the base taurine. King reported the pK_A value of the $[2\text{-Sea}]^+$ cation in an aqueous solution according to the following stepwise dissociation [11]:

$$NH_3^+(CH_2)_2SO_3H + H_2O \rightleftharpoons NH_3^+(CH_2)_2SO_3^- + H_3O^+ \qquad pK_{A1} \approx -0.33 \quad (4)$$

$$NH_3^+(CH_2)_2SO_3^- + H_2O \rightleftharpoons NH_2(CH_2)_2SO_3^- + H_3O^+ \qquad pK_{A2} = 9.05 \quad (5)$$

As is conveyed in Eq. (4), the acidity of $[2\text{-Sea}]^+$ is clearly much higher compared to most commercially-available ammonium- or imidazolium-based PILs. For instance, the pK_A of diethylmethylammonium $[Dema]^+$ and 1-ethylimidazolium $[1\text{-EIm}]^+$ cations, which are 10.35 and 7.26, respectively [12,13], indicate that the cation acidity of $[2\text{-Sea}]^+$ is much higher than $[Dema]^+$ and $[1\text{-EIm}]^+$ cations. However, pK_A values are only valid for describing proton transfer equilibria in diluted aqueous solutions. In the mass action laws corresponding to Eq. (4) and Eq. (5), the change in activity coefficients cannot be disregarded when changing to highly concentrated systems. Thus, it is of

great importance to investigate the protolytic equilibria of PILs with a low concentration of water, which could facilitate further progress in the design of PIL electrolytes for fuel cell applications.

Raman spectroscopy provides insights into the molecular structure and interactions in ILs [14]. Unfortunately, only very few investigations of PILs with strong Brønsted acidic sulfoalkylammonium cation by means of vibrational spectroscopy are to be found in the literature. This study seeks to analyze the protolysis of [2-Sea][TfO] at low water concentrations (up to 7% weight content) using Raman spectroscopy. Density functional theory (DFT) calculations were conducted to assign the vibration modes sensitive to protonation and determine the most probable cation conformation preferred in the liquid PIL.

The protolysis reaction of a strong Brønsted-acidic PIL and residual water can be quantified via the mass action law. The mass action law includes the activities a_i of all species *i*, *i.e.* the PIL cation BH^+, its conjugated base B, water, and hydroxonium ions:

$$K_\mathrm{A} = \frac{a_\mathrm{B} \cdot a_{\mathrm{H_3O^+}}}{a_{\mathrm{BH^+}} \cdot a_{\mathrm{H_2O}}} \tag{6}$$

The equilibrium constant K_A depends on the free standard reaction enthalpy $\Delta_\mathrm{R}G^0$ of the protolysis in Eq. (4). The activities a_i can be related to molar concentration c_i of species using the activity coefficient γ, where $a_i = \gamma_i\, c_i$. Thus, the relationship between the ratio of concentration and the equilibrium constant yields as:

$$K_A' = \frac{c_B \cdot c_{H_3O^+}}{c_{BH^+} \cdot c_{H_2O}} = K_\mathrm{A} \cdot \frac{\gamma_{\mathrm{BH^+}} \cdot \gamma_{\mathrm{H_2O}}}{\gamma_\mathrm{B} \cdot \gamma_{\mathrm{H_3O^+}}} \tag{7}$$

There is no simple way to consider the activity constants γ_i. The well-known Debye-Hückel limiting law is not valid for concentrations as high as treated in this study, see also the study by Edwards, investigating the protolysis equilibrium in concentrated triflic acid [15]. In an extended model for such systems, *e.g.*, the formation of ion pairs has to be considered. For the sake of simplicity, a new equilibrium constant K_A' are included, see Eq. (7). Thus, its value is only an average of the investigated concentration range, depending on the concentration dependence of the activity constants. In the following considerations, the concentrations c_i and K_A' are used.

The relationship between the initial concentration of the cations of the PIL and the initial concentration of water to the equilibrium concentrations are expressed as:

$$c^0_{\mathrm{BH^+}} = c_{\mathrm{BH^+}} + c_\mathrm{B} \tag{8}$$

$$c^0_{\mathrm{H_2O}} = c_{\mathrm{H_2O}} + c_{\mathrm{H_3O^+}} \tag{9}$$

$$\text{and} \quad c_\mathrm{B} = c_{\mathrm{H_3O^+}} \tag{10}$$

The ratio of the initial concentration of cations and water is introduced as a (dimensionless) composition parameter ξ. The ratio of the equilibrium concentration of the cations and their initial concentration is introduced as protolysis parameter α:

$$\xi = \frac{c^0_{\mathrm{H_2O}}}{c^0_{\mathrm{BH^+}}} \tag{11}$$

$$\alpha = \frac{c_{\mathrm{BH}^+}}{c^0_{\mathrm{BH}^+}} \tag{12}$$

By inserting Eq. (8) into (12) in the mass action law in Eq. (7), a quadratic relationship between the protolysis parameter α, the initial composition parameter ξ, and the equilibrium constant K_A can be derived. Depending on the value of K'_A, the following solutions can be derived for α:

$$K'_A \neq 1: \qquad \alpha = 1 + \frac{(1+\xi)K'_A}{2(1-K'_A)} \pm \sqrt{\frac{(1+\xi)K'_A}{2(1-K'_A)} + \frac{\xi K'_A}{1-K'_A}} \tag{13}$$

$$K'_A = 1: \qquad \alpha = 1 - \frac{\xi}{1-\xi} \tag{14}$$

The positive sign in Eq. (13) must be applied if $K'_A > 1$, and the negative sign if $K'_A < 1$. Thus, the equilibrium constant K'_A can be experimentally-determined by measuring the protolysis parameter α as a function of the initial composition parameter ξ.

2 Experimental section

2.1 Sample preparation

[2-Sea$^+$][TfO$^-$] was prepared as follows: 10 ml of trifluoromethanesulfonic acid (98%, Sigma Aldrich) was added dropwise to 13.9 g of 2-aminoethanesulfonic acid (taurine, ≥99%, Sigma Life Science). The mixture was stirred at 80 °C for 1 h. The clear, colorless liquid was then stored under dry conditions to prevent water absorption. The water content was determined via Karl-Fischer titration and found to be 0.4 wt%, and was referred to hereinafter as a "neat" ionic liquid. The neat ionic liquid was diluted with aliquot amounts of water in order to obtain a series of samples with water contents ranging from 1 wt% to 7 wt%. To ensure the stoichiometric composition of the prepared PIL, a N/S elementary analysis (ICP-MS) and an acid-base titration were performed (details in Fig.S1). The deviation regarding an excess of trifluoromethanesulfonic acid or of taurine is estimated to be less than 1–2 mol%.

2.2 Raman measurements

The Raman spectra were recorded using a diode laser (Oxxius Laserboxx LBX-785S100-CIR-PP) with a wavelength λ = 785 nm for excitation. The Rayleigh scattering signal at the laser wavelength was blocked by a thin film interference filter. A microscope objective was to direct the beam to a quartz cuvette with the sample and collect the back-scattered light (Zeiss EC Epiplan 10x/0.2 M27; working distance: 14.3 mm; NA: 0.2; parfocal length: 45.0 mm). The scattered light was directed to a spectrograph via a dichroic mirror and a plano-convex lens (Andor Shamrock SR-303i-A, f/4, Czerny-Turner arrangement, diffraction grating: 1200 lines/mm). A back-illuminated CCD camera was used to record the signal (Andor iKonM 934, 1024x1024 pixels, Peltier-cooled to −60 °C). For the used setup and an entrance slit of 40 µm, the spectral resolution was about 2 cm^{-1}. Raman spectra were collected from both the neat [2-Sea][TfO] and diluted series. The spectra were background subtracted due to an appreciable fluorescence background. The spectra of a diluted (50 mol%) aqueous solution of CF_3SO_3H and a saturated aqueous solution of taurine were then collected for comparison.

2.3 Theoretical calculations

DFT calculations on the B3LYP level (VWN5) were performed, in combination with a polarizable continuum model (PCM). Using the ab initio quantum chemistry package (US-)GAMESS (2013 R1), a geometric optimization and an analysis of the vibrational frequencies were carried out for the most probable conformers of the cation and anion (OPTTOL = 1e-05, NCONV = 6) [16]. The split-valence basis set 6-311++G(3df,2p) was used to take account on the d-type orbitals of the sulfur atom and on the diffuse s and l shells of hydrogen and the heavy atoms. In a second run, the Raman intensities were calculated to obtain spectral data for [2-Sea][TfO].

The polarizable continuum model was used to take the dielectric environment of the ions into account. Due to a lack of data for the relative dielectric constant ε_r of the surrounding medium, the default model of water was chosen for all reported calculations, *i.e.* an ε_r of 78. In the case of a highly acidic sulfonic acid-based PIL, it is reasonable to assume a high ε_r value in the range between 50 and 100. Values of 61 for neat H_3PO_4 and 101 for neat H_2SO_4 can be found in the literature [17–19].

When analyzing the conformational degree of freedom of the $[2\text{-Sea}]^+$ cation, the free energy should primarily depend on the rotational conformation of the CC bond. A ring-like CC-*gauche* and an open-chain CC-*trans* conformation can be distinguished, due to the mutual orientation of the NH_3^+ and SO_3H group; see Fig. 2. According to Ohno et al., the CC-*gauche* conformation prevails in aqueous solutions [20]. Apparently, the presence of an internal H bond reduces the free energy. The free energy in the $[2\text{-Sea}]^+$ cation should also depend to a lesser extent on the orientation of the OH group. Thus, according to the mutual orientation of the NH_3^+ and SO_3H group, one must also distinguish an SC-*gauche* and SC-*trans* conformation, which will result in four conformers being considered in the calculations, *i.e.* $[2\text{-Sea}]^+$ (g,g), (g,t), (t,g), and (t,t).

3 Results and discussion

3.1 Raman spectra of neat [2-Sea][TfO] and [2-Sea][TfO] with 7 wt% H_2O

Fig. 1 displays the experimental spectra of neat [2-Sea][TfO], [2-Sea][TfO] + 7 wt% H_2O in comparison to a saturated aqueous solution of taurine and a diluted aqueous solution of CF_3SO_3H (50 mol%). The peaks of a saturated aqueous solution of taurine, marked by blue dotted lines, are consistent with the reported spectra of taurine [20,21]. The vibrational bands observed in the spectrum of CF_3SO_3H solution are assigned on the basis of the previous studies [22–24], as marked by the black dotted lines in Fig. 1. In the spectrum of neat [2-Sea][TfO], the four most intense Raman bands at 319, 350, 768, and 1033 cm^{-1} are assigned to ν(SC), $\rho(SO_3)$, $\delta_s(CF_3)$ and $\nu_s(SO_3)$. In turn, the weak and medium bands located at 517, 576, 1188, and 1232 cm^{-1} are assigned to $\delta_{as}(SO_3)$, $\delta_{as}(CF_3)$, $\nu_{as}(SO_3)$ and $\nu_s(CF_3)$ of the $[TfO]^-$ anion. The positions correspond well with the findings from the aqueous solution of CF_3SO_3H and with other experimental studies on the aqueous solutions of alkali triflates and triflate-based ionic liquids [22–25]. The other Raman bands in the spectrum of neat [2-Sea][TfO] at 448, 500, 589, 728, 783, 836, 881 and 1163 cm^{-1} in Fig. 1 are supposed to stem from the $[2\text{-Sea}]^+$ cation. Most of these bands are weak, expect the prominent bands at 500, 728

and 1164 cm^{-1}. The medium-intensity Raman band at 500 cm^{-1} has an obvious shoulder at 483 cm^{-1}. Meanwhile, the weak band at 209 cm^{-1} is relatively broader and may constitute a superposition of an anion and a cation band.

The mixture of [2-Sea][TfO] with 7 wt% water exhibits fairly similar peak positions compared to the neat PIL. However, a complex change is apparent in the broad band at around 500 cm^{-1} and an upward shift of the medium peak at 728 cm^{-1} to 735 cm^{-1}. In the spectra of the saturated aqueous solution of taurine shown in Fig. 1, a peak at about 735 cm^{-1} is also observed. According to the study by Ohno et al., this peak is assigned to the ν(SC) stretching mode of taurine [20].

3.2 DFT calculation of the Raman spectra

In order to support the evaluation of the spectroscopic data, DFT calculations were performed using the software GAUSSUM [26]. The calculated Raman activities ($Å^4$ amu^{-1}) shown in Table 1 and Table 2 and in the supplementary material were converted into Raman intensities for the experimental excitation wavelength of 785 nm and a temperature of 25 °C. Fig. 2 depicts the relative Raman intensities of the $[2\text{-Sea}]^+$ (g,g), (g,t), (t,g), and (t,t) conformers, each of which is superposed with the Raman intensity of the $[TfO]^-$ anion.

Conformations

The $[TfO]^-$ anion has a C_{3v} symmetry. There is an energy barrier impeding the rotation of the CF_3 and SO_3 groups, and therefore only the staggered conformation can be found. According to the calculations, the free energy of the eclipsed conformation is in the order of 12 kJ mol^{-1} higher than the staggered conformation. The calculated values for the bond lengths and angles are summarized in the supplementary material (see the normal coordinates). The values deviate from the literature data reported for other ILs with $[TfO]^-$ anions by only 0.5–2% [27].

The four probable $[2\text{-Sea}]^+$ cation conformers were analyzed by DFT, as shown in Fig. 2. The free energy of both of the CC-*gauche* conformers $[2\text{-Sea}]^+$ (g,g) and $[2\text{-Sea}]^+$ (g,t) is significantly lower compared to the open-chain CC-*trans* conformers $[2\text{-Sea}]^+$ (t,t) and $[2\text{-Sea}^+]$ (t,g). According to the calculations, $[2\text{-Sea}]^+$ (g,g) is the most stable conformer.

Vibrational analysis

Anharmonicity effects are neglected and polarization may not be sufficiently taken into account in this DFT study. The former are the origin of an overestimation of the vibration frequencies in the high-frequency range above 1800 cm^{-1}, whereas the latter can cause an underestimation of low vibration frequencies below 1800 cm^{-1} [28,29]. Therefore, a scaling factor of 1.02 for both the anion and cation was introduced, which results in the best match between the experimentally- and DFT-calculated Raman spectra.

The calculated vibration frequencies and Raman activities of the $[TfO]^-$ anion are compiled in Table 1. 18 vibration modes were obtained, corresponding to the number of atoms of the $[TfO]^-$ anion. The assignments of the vibration modes shown in Table 1

was performed by only considering only the internal coordinates, whose energy contributions distinctly predominate in the potential energy distribution (PED). Only energy contributions of internal coordinates above 5% were considered. The assignments in Table 1 are also in agreement with the results of Miles et al., Huang et al., Frech et al., Schwenzer et al. and Singh. et al. [22–25]. Only the assignment of the Raman band at 1188 cm^{-1} is ambiguous. As is shown in Fig. 2, the most intensive peaks of [2-Sea][TfO] are contributed by the $[TfO]^-$ anion. A good match between the calculated $[TfO]^-$ vibration modes and the experimental Raman bands was obtained for a scaling factor of 1.02, with deviations in the range of 5–10 cm^{-1}, except for the Raman band at 319 cm^{-1}, which was approximately 20 cm^{-1} higher than the calculated frequency.

Among the four conformers of the $[2\text{-Sea}]^+$ cation, the calculated vibration spectrum of the $[2\text{-Sea}]^+$ (g,g) conformer presents the best agreement for the experimental Raman spectra, as is shown in Fig. 2. The medium Raman band at 728 cm^{-1} and the broad and complex weak band at about 500 cm^{-1} are characteristic of the cation. Table 2 shows the calculated vibration frequencies for the $[2\text{-Sea}]^+$ (g,g) conformer. The calculated vibration frequencies for the other conformers can be found in the supplemental material. According to the calculations, the $\delta(SO_2)$ and $\delta(SO_2) + \delta(NCC)$ deformations mode of the (g,g) conformer can be found at 493 and 468 cm^{-1}. The analogue vibration modes for taurine, $\delta_s(SO_3)$, and $\delta(NCC) + \delta_s(SO_3)$, were observed by Ohno et al. at 526 and 458 cm^{-1} [20]. Therefore, the weak Raman band at 500 cm^{-1} and its shoulder at 483 cm^{-1} in the experimental Raman spectra could most likely be assigned to a deformation mode of the SO_3H moiety.

The calculated frequencies of the ν(SC) vibration mode for the ring-like CC-*gauche* conformations were lower than that of the CC-*trans* conformations. The calculated ν(SC) vibration was found at 727 cm^{-1} for the (g,g) conformer and 716 cm^{-1} for the (g,t) conformer, whereas it occurred at 776 cm^{-1} for the (t,t) and 761 cm^{-1} for the (t,g) conformer. In the experimental spectra of neat [2-Sea][TfO] shown in Fig. 2, a medium peak can be observed at 728 cm^{-1}. This indicates that the ring-like CC-*gauche* conformations of the $[2\text{-Sea}]^+$ cation are more prevalent in the ionic liquid [2-Sea][TfO] than CC-*trans* conformations. It was reported by Ohno et al. that the CC-*gauche* conformation also prevails in an aqueous solution of taurine [20]. However, it is difficult to determine whether the (g,g) or (g,t) conformers prevail in the [2-Sea][TfO]. The (g,g) conformers better resemble the experimentally-observed broad and complex band at 500 cm^{-1}, and it also has the lowest free energy. In the case of the (g,t) conformer, only one Raman band at 508 cm^{-1} is present.

3.3 Protolytic equilibrium of [2-Sea][TfO] and residual water

The protolysis reaction of the strong Brønsted-acidic [2-Sea][TfO] and residual water is investigated by varying the mass fractions of the ionic liquid w_{SeaTfO}, respectively of water $w_{\mathrm{H_2O}}$. Samples consist of [2-Sea][TfO] and aliquot amounts of water with mass fractions from 0.4 wt% to 7 wt% (5.8 mol% to 53.5 mol%) water. Essentially, there is only a protolytic equilibrium between the $[2\text{-Sea}]^+$ cation and water in the PIL–H_2O binary system, as shown in the following equation:

$$NH_3^+(CH_2)_2SO_3H + TfO^- + H_2O \rightleftharpoons NH_3^+(CH_2)_2SO_3^- + H_3O^+ + TfO^- \qquad (15)$$

The $[TfO]^-$ anion is not involved in any protolysis equilibrium with water due to its very low basicity. [2-Sea][TfO]–H_2O is regarded as a binary system.

The Raman spectra in the region between 680–870 cm^{-1} of neat [2-Sea][TfO] and of mixtures consisting of [2-Sea][TfO] with water are depicted in Fig. 3(a). We assume that the corresponding Raman band intensities of the $[TfO]^-$ anion should not change when adding only a small amount of water. Thus, the spectra were normalized with respect to the intensity of the $\delta_s(CF_3)$ band located at 768 cm^{-1}, which is the most intense band in the range of 500–1500 cm^{-1}. According to the considerations above, the $[2\text{-Sea}]^+$ cation and taurine are most likely present in a CC-*gauche* conformation. The ν(SC) vibration modes of $[2\text{-Sea}]^+$ (g,g) appear at 728 cm^{-1}, and of taurine (g) at 739 cm^{-1}. The protonation of the adjacent SO_3^- group results in a shift of about 11 cm^{-1} to lower wavenumbers. The two Raman bands partially overlap, resulting in a broad peak with a distinct shoulder when increasing the water content. Using Voigt functions for the peak deconvolution of the ν(SC) vibration modes of $[2\text{-Sea}]^+$ and taurine, as well as of the $\delta_s(CF_3)$ bending mode of the anion results in very small Lorentz components in comparison to the Gaussian components. Hence, the Raman spectra were fitted by using only Gaussian peak functions to deconvolute the peaks in the spectral region between 680–870 cm^{-1}. As is depicted in Fig. 3(c), the peak position obtained from fitting does not depend on the H_2O content, *i.e.*, the fit procedure is stable. This reveals that the intensity of the deconvoluted peak at 728 cm^{-1} decreases with the addition of water, whereas the peak at 739 cm^{-1} is increasing; see Fig. 3(b). This confirms the deprotonation of the SO_3H group of the $[2\text{-Sea}^+]$ cations with increasing H_2O content, and the presence of the conjugated base taurine in the equilibrium. The normalized integral intensities can be utilized to monitor the protolysis.

The normalized integral intensity I_{728} of the band at 728 cm^{-1} should be proportional to the equilibrium concentration c_{BH^+} of the $[2\text{-Sea}]^+$ cation. Meanwhile, the normalized integral intensity I_{739} of the band at 739 cm^{-1} should be proportional to the equilibrium concentration c_B of the conjugated base taurine. When neglecting again the change in intensity when adding only small amounts of water, the protolysis parameter α in Eq. (12) can be expressed by the ratio of the normalized integral intensities I_{728} at a certain H_2O content w_{H_2O} and for the neat PIL ($w_{H_2O} = 0$):

$$\alpha = \frac{c_{\mathrm{HB}^+}}{c^0_{\mathrm{HB}^+}} = \frac{c_{\mathrm{Sea}^+}}{c^0_{\mathrm{Sea}^+}} = \frac{I_{728}(w_{\mathrm{H_2O}})}{I_{728}(w_{\mathrm{H_2O}}=0)} \tag{16}$$

The composition parameter ξ in Eq. (11), *i.e.* the ratio of the initial concentrations of the cations $c^0_{Sea^+}$ ($\equiv c^0_{SeaTfO}$) and water $c^0_{H_2O}$, can be calculated from the mass fraction of water w_{H_2O}, according to Eq. (17). The precise value of w_{H_2O} in the samples can be determined by Karl-Fischer titration.

$$\xi = \frac{c^0_{\mathrm{H_2O}}}{c^0_{\mathrm{Sea}^+}} = \frac{M_{\mathrm{SeaTfO}}}{M_{\mathrm{H_2O}}} \frac{m^0_{H_2O}}{m^0_{SeaTfo}} = \frac{M_{\mathrm{SeaTfO}}}{M_{\mathrm{H_2O}}} \frac{w_{\mathrm{H_2O}}}{1-w_{\mathrm{H_2O}}} \tag{17}$$

In Fig. 4, the spectroscopically-determined protolysis parameter α is plotted as a function of the composition parameter ξ. Using Eq. 7. to fit the data, this yields a value of 0.23 ± 0.09 for K'_A (25 °C).

The error of K'_A of about ±50% is appreciably high. The scattering of the data is supposed to be caused by the limitations of spectroscopic measurements as well as by the data analysis procedure. In particular, the intensity of the Raman band of the neat sample was used for normalization, which increases the relative errors especially for low water fractions. *E.g.*, as the normalized integrated intensity of I_{728}/I_{768} at a water fraction of 1 wt% is slightly larger than that of neat sample in Fig.3 (b), this leads to an outlier at $\xi = 0.15$ in Fig. 4. A possible non-stoichiometry of the PIL had been checked but found not to be a responsible reason for the errors. An acid or base excess is determined to be only in the range of 1–2 mol% (details in Fig.S1). An acid excess of *e.g.* 2 mol% would correspond to ~2 mol% of additional water necessary to deprotonate the excess TfOH. In terms of the composition parameter ξ, this would produce an error of 0.02 at maximum and thus is far beyond the detection limits. Moreover, concentrations were used to describe the equilibrium constant. Possible variations of the activity constants have not been taken into account and might lead to systemic derivations.

To our best knowledge, there is only one experimental measurement on the pK_A of protonated taurine, *i.e.*, [2-Sea]$^+$ cations. In this study, the pK_A value is estimated from measurements in an aqueous solution by explicitly considering the levelling effect of water. A pK_A value of −0.33 was reported [11]. This corresponds to a K_A value of 2.1. A pK_A acidity value is defined for an ideal diluted aqueous solution, *i.e.*, for a constant water activity a_{H_2O} of approximate unity. This may explain the fact that the measured value for the PIL–H_2O system in the case of only small amounts of water is significantly lower, as it can be considered as a solution of water in a salt melt. The activity of the water and the activity coefficients of the ionic species are far from unity, which leads to the deviation of the equilibrium constant. However, the K'_A value of [2-Sea]$^+$ cation is found to be in the same order of magnitude as H_3O^+. This indicates that the acidity/proton donor activity of the [2-Sea]$^+$ cations is comparable to that of the hydroxonium ions. The high acidity of the [2-Sea]$^+$ cation implies fast proton exchange processes between the PIL cations and water molecules. An increasing share of cooperative proton transport was found in a previous study when increasing the water content from 0.4 wt% to 5.7 wt%. (1:1 molar ratio PIL:H_2O) [8]. According to the measured protolysis constant value, about 30% of the sulfoalkylammonium cations transfer their proton to the water molecules. A high proton donor activity is beneficial for the ORR at the electrode interface. This indicates that PILs with sulfoalkylammonium cations are promising candidates to be used as electrolytes in future fuel cells operating above 100 °C.

4 Summary

By using Raman spectroscopy, the protolysis of a high Brønsted acidic PIL [2-Sea][TfO] was measured in highly concentrated systems, *i.e.*, in the presence of an only small amount of water with a concentration of up to 7 wt%. DFT calculations were carried out to investigate the conformations of the [2-Sea]$^+$ cation and identify the peaks of the Raman spectra. The four most probable conformers of the cation were considered, depending on the rotational positions of the CC and SC bond. The best match of the calculated spectra to the experimental was found for the CC-*gauche* conformations. This suggests an annular conformation with an internal H-bond between the NH_3^+ and SO_3H group.

A characteristic frequency shift of the ν(SC) stretching vibration was observed with the addition of water in [2-Sea][TfO]. The broad band could be deconvoluted into two peaks at 728 cm^{-1} and 739 cm^{-1}. The intensity of the peak at 739 cm^{-1}, related to the concentration of the neutral taurine was increasing with increasing water content. The intensity of the peak at 728 cm^{-1}, which corresponds to the concentration of the protonated cation $[2\text{-Sea}]^+$, decreases with increasing water content in the PIL. For a quantitative analysis of the proton transfer, a protolysis equilibrium constant was calculated by fitting the function of the protolysis parameter α and the initial composition parameter ξ. This yields a value of $K'_A = 0.23 \pm 0.09$ for [2-Sea][TfO] (assuming constant activities coefficients). The acidity is comparable to that of hydroxonium cations. Former investigations have indicated that the presence of a strong proton donor is necessary to avoid a high activation overvoltage due to a slow ORR kinetics. Thus, this PIL is a promising non-aqueous electrolyte for future fuel cell application, due to its strong proton donor abilities.

Acknowledgments

The authors are grateful for the support of the Helmholtz Association. Y. Chen acknowledges the financial support by the Federal Ministry for Economic Affairs and Energy of Germany (HiFi-PEFC, Project No. 03ETB003A).

References

[1] Q. Li, J.O. Jensen, R.F. Savinell, N.J. Bjerrum, High temperature proton exchange membranes based on polybenzimidazoles for fuel cells, Progress in Polymer Science 34 (2009) 449–477. https://doi.org/10.1016/j.progpolymsci.2008.12.003.

[2] J.-T. Wang, R.F. Savinell, J. Wainright, M. Litt, H. Yu, A fuel cell using acid doped polybenzimidazole as polymer electrolyte, Electrochimica Acta 41 (1996) 193–197. https://doi.org/10.1016/0013-4686(95)00313-4.

[3] J.S. Wainright, J.-T. Wang, D. Weng, R.F. Savinell, M. Litt, Acid-Doped Polybenzimidazoles: A New Polymer Electrolyte, J. Electrochem. Soc. 142 (1995) L121-L123. https://doi.org/10.1149/1.2044337.

[4] A. Noda, M.A.B.H. Susan, K. Kudo, S. Mitsushima, K. Hayamizu, M. Watanabe, Brønsted Acid−Base Ionic Liquids as Proton-Conducting Nonaqueous Electrolytes, J. Phys. Chem. B 107 (2003) 4024–4033. https://doi.org/10.1021/jp022347p.

[5] A.S. Amarasekara, Acidic Ionic Liquids, Chemical reviews 116 (2016) 6133–6183. https://doi.org/10.1021/acs.chemrev.5b00763.

[6] K.-D. Kreuer, A. Rabenau, W. Weppner, Vehicle Mechanism, A New Model for the Interpretation of the Conductivity of Fast Proton Conductors, Angew. Chem. Int. Ed. Engl. 21 (1982) 208–209. https://doi.org/10.1002/anie.198202082.

[7] K. Wippermann, J. Giffin, C. Korte, In Situ Determination of the Water Content of Ionic Liquids, J. Electrochem. Soc. 165 (2018) H263-H270. https://doi.org/10.1149/2.0991805jes.

[8] J. Lin, L. Wang, T. Zinkevich, S. Indris, Y. Suo, C. Korte, Influence of residual water and cation acidity on the ionic transport mechanism in proton-conducting ionic liquids, Physical chemistry chemical physics PCCP 22 (2020) 1145–1153. https://doi.org/10.1039/c9cp04723a.

[9] H. Hou, H.M. Schütz, J. Giffin, K. Wippermann, X. Gao, A. Mariani, S. Passerini, C. Korte, Acidic Ionic Liquids Enabling Intermediate Temperature Operation Fuel Cells, ACS applied materials & interfaces 13 (2021) 8370–8382. https://doi.org/10.1021/acsami.0c20679.

[10] K. Wippermann, J. Wackerl, W. Lehnert, B. Huber, C. Korte, 2-Sulfoethylammonium Trifluoromethanesulfonate as an Ionic Liquid for High Temperature PEM Fuel Cells, Journal of The Electrochemical Society 163 (2015) F25-F37. https://doi.org/10.1149/2.0141602jes.

[11] E.J. King, The Ionization Constants of Taurine and its Activity Coefficient in Hydrochloric Acid Solutions from Electromotive Force Measurements, J. Am. Chem. Soc. 75 (1953) 2204–2209. https://doi.org/10.1021/ja01105a053.

[12] W.M. Haynes, CRC handbook of chemistry and physics, CRC Press, Boca Raton, 2016.

[13] B. Lenarcik, P. Ojczenasz, The influence of the size and position of the alkyl groups in alkylimidazole molecules on their acid-base properties, Journal of Heterocyclic Chemistry 39 (2002) 287–290. https://doi.org/10.1002/jhet.5570390206.

[14] V.H. Paschoal, L.F.O. Faria, M.C.C. Ribeiro, Vibrational Spectroscopy of Ionic Liquids, Chemical reviews 117 (2017) 7053–7112. https://doi.org/10.1021/acs.chemrev.6b00461.
[15] H. Edwards, The vibrational spectrum of trifluoromethanesulphonic acid, CF_3SO_3H, and the determination of its degrees of dissociation in aqueous solution by Raman spectroscopy, Spectrochimica Acta Part A: Molecular Spectroscopy 45 (1989) 715–719. https://doi.org/10.1016/0584-8539(89)80257-0.
[16] G.M.J. Barca, C. Bertoni, L. Carrington, D. Datta, N. de Silva, J.E. Deustua, D.G. Fedorov, J.R. Gour, A.O. Gunina, E. Guidez, T. Harville, S. Irle, J. Ivanic, K. Kowalski, S.S. Leang, H. Li, W. Li, J.J. Lutz, I. Magoulas, J. Mato, V. Mironov, H. Nakata, B.Q. Pham, P. Piecuch, D. Poole, S.R. Pruitt, A.P. Rendell, L.B. Roskop, K. Ruedenberg, T. Sattasathuchana, M.W. Schmidt, J. Shen, L. Slipchenko, M. Sosonkina, V. Sundriyal, A. Tiwari, J.L. Galvez Vallejo, B. Westheimer, M. Włoch, P. Xu, F. Zahariev, M.S. Gordon, Recent developments in the general atomic and molecular electronic structure system, The Journal of Chemical Physics 152 (2020) 154102. https://doi.org/10.1063/5.0005188.
[17] R.A. MUNSON, Dielectric Constant of Phosphoric Acid, J. Chem. Phys. 40 (1964) 2044.
[18] R.J. Gillespie, R.H. Cole, The dielectric constant of sulphuric acid, Trans. Faraday Soc. 52 (1956) 1325. https://doi.org/10.1039/tf9565201325.
[19] R.A. Munson, Self-Dissociative Equilibria in Molten Phosphoric Acid (1964).
[20] K. Ohno, Y. Mandai, H. Matsuura, Vibrational spectra and molecular conformation of taurine and its related compounds, Journal of Molecular Structure 268 (1992) 41–50. https://doi.org/10.1016/0022-2860(92)85058-O.
[21] N. Maiti, S. Thomas, A. Debnath, S. Kapoor, Raman and XPS study on the interaction of taurine with silver nanoparticles, RSC Adv. 6 (2016) 56406–56411. https://doi.org/10.1039/C6RA09569K.
[22] B. Schwenzer, S.N. Kerisit, M. Vijayakumar, Anion pairs in room temperature ionic liquids predicted by molecular dynamics simulation, verified by spectroscopic characterization, RSC Adv. 4 (2014) 5457. https://doi.org/10.1039/c3ra46069j.
[23] M.G. Miles, G. Doyle, R.P. Cooney, R.S. Tobias, Raman and infrared spectra and normal coordinates of the trifluoromethanesulfonate and trichloromethanesulfonate anions, Spectrochimica Acta Part A: Molecular Spectroscopy 25 (1969) 1515–1526. https://doi.org/10.1016/0584-8539(69)80135-2.
[24] R. Frech, W. Huang, Anion-solvent and anion-cation interactions in lithium and tetrabutylammonium trifluoromethanesulfonate solutions, J Solution Chem 23 (1994) 469–481. https://doi.org/10.1007/bf00972613.
[25] D.K. Singh, B. Rathke, J. Kiefer, A. Materny, Molecular Structure and Interactions in the Ionic Liquid 1-Ethyl-3-methylimidazolium Trifluoromethanesulfonate, The journal of physical chemistry. A 120 (2016) 6274–6286. https://doi.org/10.1021/acs.jpca.6b03849.

[26] N.M. O'Boyle, A.L. Tenderholt, K.M. Langner, cclib: a library for package-independent computational chemistry algorithms, J. Comput. Chem. 29 (2008) 839–845. https://doi.org/10.1002/jcc.20823.
[27] J.L. Bourque, K.M. Baines, Tetramethylammonium trifluoromethanesulfonate, IUCrData 1 (2016) 8307. https://doi.org/10.1107/S2414314616003709.
[28] M.D. Halls, J. Velkovski, H.B. Schlegel, Harmonic frequency scaling factors for Hartree-Fock, S-VWN, B-LYP, B3-LYP, B3-PW91 and MP2 with the Sadlej pVTZ electric property basis set, Theoretical Chemistry Accounts 105 (2001) 413–421. https://doi.org/10.1007/s002140000204.
[29] J.P. Merrick, D. Moran, L. Radom, An evaluation of harmonic vibrational frequency scale factors, The journal of physical chemistry. A 111 (2007) 11683–11700. https://doi.org/10.1021/jp073974n.

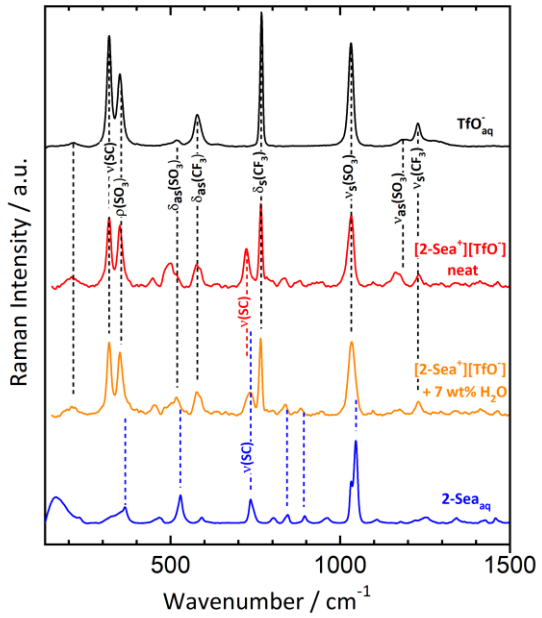

Fig. 1. Raman spectra of: a) a diluted aqueous solution of trifluoromethanesulfonic acid [TfO^-], neat [2-Sea^+][TfO^-], [2-Sea^+][TfO^-] with 7 wt% of H_2O, and a diluted aqueous solution of taurine [2-Sea].

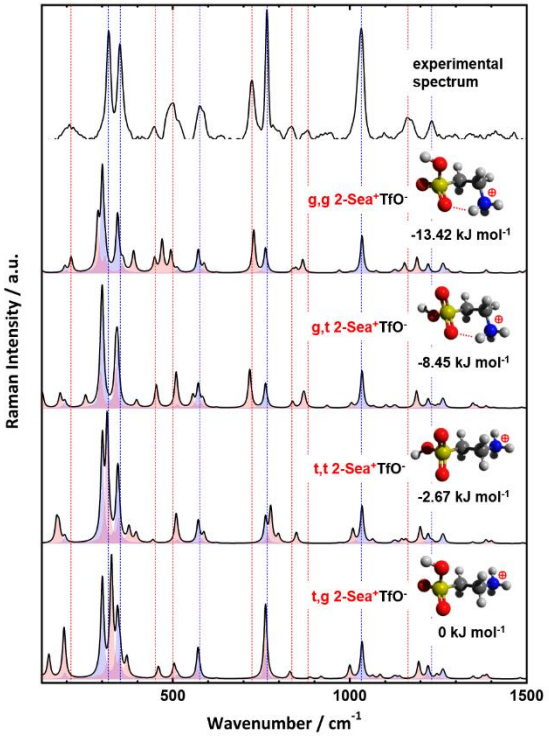

Fig. 2. Simulated Raman spectra of the conformers [2-Sea^+] (g,g) and (g,t) and (b) of [2-Sea^+] (t,g) and (t,t), each superposed with the calculated spectrum of the [TfO^-], in comparison to the experimental Raman spectrum of neat [2-Sea^+][TfO^-].

Table 1. Vibration modes of the [TfO^-], from the DFT calculations on the B3LYP level with the basis set 6-31+G(d,p) and the PCM model for water as a solvent.

Wavenumbers /cm^{-1}	Å^4 /amu	Vibration modes of [TfO^-]
71	0.00	τ(OS-CF)
194	0.07	ρ(SO_3) + ρ(CF_3)
300	5.09	ν(SC)
342	2.06	ρ(CF_3) + ρ(SO_3)
344	2.05	
511	0.31	δ_{as}(SO_3) + δ_{as}(CF_3)
513	0.31	
571	2.35	δ_{as}(CF_3) + δ_{as}(SO_3)
572	2.38	
623	0.17	δ_s(SO_3)
761	9.44	δ_s(CF_3)+ ν(SC)
1034	28.82	ν(SO_3)
1124	1.77	ν_{as}(CF_3)
1130	1.76	
1221	10.05	ν_s(CF_3) + ν(SC)
1261	6.80	δ_{as}(SO_3)
1265	6.73	

Table 2. Vibration modes of the [2-Sea^+] from the DFT calculations on the B3LYP level with the basis set 6-31+G(d,p) and the PCM model for water as a solvent.

Wavenumbers /cm^{-1}	Å^4 /amu	Vibration modes of [2-Sea^+] (g,g)
120	0.09	τ(OS-CC)
211	0.39	δ(SCC) + τ(SO_2)
287	2.24	τ(SO_2) + δ(NCC)
308	0.76	δ(C-S-OH) + τ(SC-CN)
358	0.71	τ(CS-OH)
388	1.88	τ(SC-CN) + δ(NCC) + δ(SCC)
447	1.68	δ(O-S-OH) + δ(NCC)
468	4.31	δ(SO_2) + δ(NCC)
493	3.20	δ(SO_2)
587	1.77	ω(SO_2)+ δ(SCC)
727	14.85	ν(SC) + ν(S-OH)
837	1.59	τ(NH3) + ν(S-OH)
847	2.04	
866	6.81	ν(NC) + ν(S-OH)
969	1.79	ν(CC) + ν(NC) + ρ ($C^{\alpha}H_2$)
1001	0.63	ρ ($C^{\beta}H_2$) + ρ ($C^{\alpha}H_2$)
1074	1.49	ν(CC) + ν(NC)
1145	1.18	δ(S-O-H) +τ($C^{\alpha}H_2$) + τ(NH_3)
1154	9.45	δ(S-O-H) + ν(SO)
1189	16.53	ν_s(SO_2) + δ(S-O-H)
1276	3.17	τ($C^{\alpha}H_2$) + ρ(NH_3)
1311	2.07	ω($C^{\alpha}H_2$) + ρ(NH_3) + ν(SO)
1384	4.79	ν_{as}(SO_2)
1426	0.76	ρ(NH_3) + τ($C^{\beta}H_2$)
1479	3.00	δ(C^{α}-C^{β}-H) + ρ($N^{\alpha}H_3$)
1497	4.63	δ($C^{\alpha}H_2$)
1573	4.51	δ($C^{\beta}H_2$)
1736	1.63	ω($C^{\beta}H_2$)
1760	1.60	δ_S(NH_3)
1942	4.30	
1956	4.49	δ_{as}(NH_3)
3145	99.45	ν($C^{\alpha}H_2$)
3200	68.81	ν_s($C^{\beta}H_2$) + ν_{as}($C^{\alpha}H_2$)
3207	100.60	
3260	35.00	ν_{as}($C^{\beta}H_2$)
3412	63.07	ν(NH)
3554	62.23	ν_s(NH_2)
3590	30.45	ν_{as}(NH_2)
3788	76.54	ν(OH)

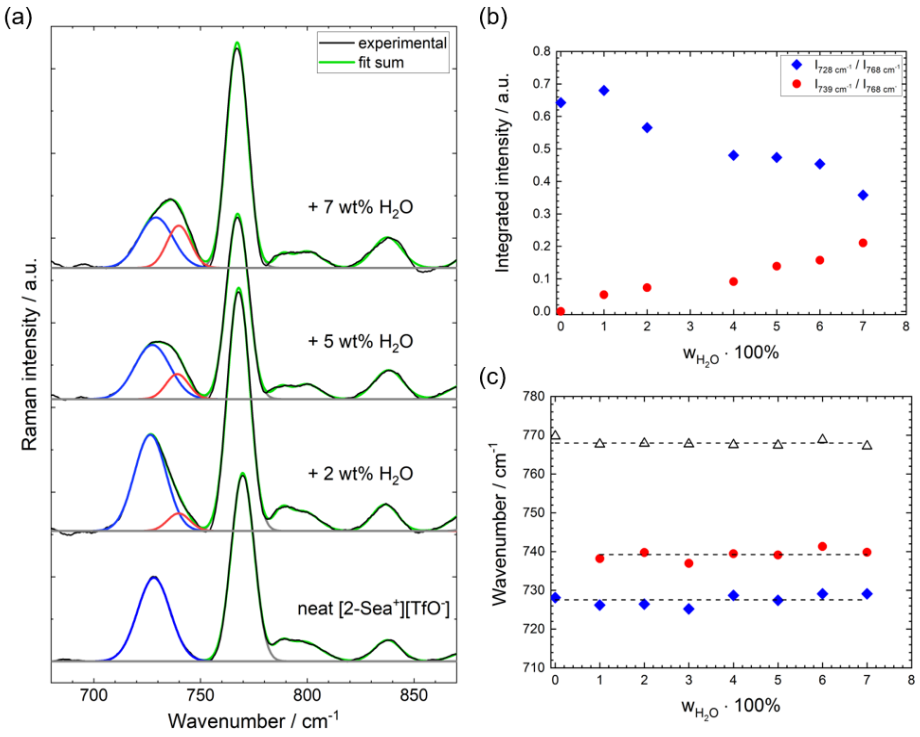

Fig. 3. (a) Raman spectra of [2-Sea$^+$][TfO$^-$] with different amounts of water in the range between 680 and 860 cm^{-1}. The experimental curves indicated in black and the fittings in green. The blue, red and gray lines represent the deconvoluted Gaussian function components; (b) normalized integral Raman intensities of the ν(CS) vibration modes as a function of the water content; and (c) peak positions of vibrations as a function of the water content.

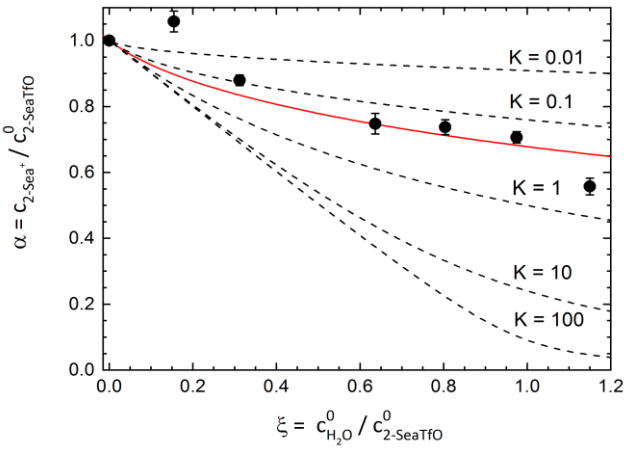

Fig. 4. Protolysis parameter α as a function of the composition ξ.